Experiments on Pultruded FRP Beam-to-column Joints: Failure Mode Analysis and Stiffness Determination

Sivaganesh SELVARAJ[1], Tak-Ming CHAN[2]* and Ben YOUNG[3]

[1]Research Assistant Professor, Department of Civil and Environmental Engineering, The Hong Kong Polytechnic University, Hong Kong, China. Email: sivaganesh.selvaraj@polyu.edu.hk

[2]*Professor, Department of Civil and Environmental Engineering, The Hong Kong Polytechnic University, Hong Kong, China. Email: tak-ming.chan@polyu.edu.hk (corresponding author)

[3]Professor, Department of Civil and Environmental Engineering, The Hong Kong Polytechnic University, Hong Kong, China. Email: ben.young@polyu.edu.hk

Abstract

The design of pultruded fiber-reinforced polymer (PFRP) structures can be considered to be governed by the beam-to-column joints as they exhibit brittle behavior. This study investigates the failure modes, stiffness contributions, and load transfer of the connection components in the PFRP beam-to-column joint made from glass pultruded structural shapes. Ten full-scale joint tests were carried out, including parameters such as three different end distances, cleat thicknesses, and additional T-stiffeners. The conventional beam-to-column joints without additional stiffeners failed in a brittle manner initiated by flange cleats followed by progressive stiffness reduction leading to ultimate failure. The analysis using strain data confirmed that there is a need for an additional load transfer component in the top flange to delay the brittle failure. The use of T-stiffeners significantly increased the initial stiffness of the beam-to-column joint and delayed the first failure. The overall rotational stiffness of the PFRP beam-to-column joint was determined using the joint component method in the Eurocode. It is shown that the Eurocode method is conservative for connection components with higher end distances. The appropriateness of the stiffness prediction method in the Eurocode is demonstrated with a design example.

Keywords: FRP Structures; Pultruded composite forms; Beam-to-column joints; First failure concept; Stiffness Determination;

Introduction

The structural fiber composite forms are called pultruded fiber-reinforced polymer (PFRP) profiles, mostly they are made of lightweight E-glass or carbon fibers with a resin matrix (EXTREN 1989 and Fiberline 1995). Interest has been increasing to use of PFRPs in construction (Clarke 1991, El-Badry 1996, Bank 2023) due to the high strength-to-weight ratio and durability against corrosive environments. In contrast to this, the brittle failure modes of PFRPs are the main drawback that needs to be addressed. Towards this objective, the beam-to-column joints for frames constructed with PFRP I-section and tubular form profiles have been investigated largely and they fail in a brittle manner thus governing the design of the entire PFRP structure. For design purposes, beam-to-column joints in frames are assumed to exhibit either nominally pinned or fully rigid behavior, but in reality, all joints behave between these two extreme assumptions. The joint's characteristics can be described by its moment-rotation relationship or stiffness (BS EN 1993-1-8:2005). Knowledge of the structural response and failure mode is necessary for the design of PFRP structural joints as they behave complicatedly in a combination of failure modes. Full-scaled physical testing is the method usually adopted to determine the characteristics of pultruded frame joints and to observe the load transfer paths. A detailed review of research on pultruded frame joints and members is available in the literature (ASCE 2011, Ellingwood 2003, Mottram and Zheng 1996; 1999a; 199b, Gand et al. 2013; Nguyen et al. 2013, 2014 and 2015, Qureshi and Mottram 2013;2014;2015, Martins et al. 2017;2021a; 2021b and 2022c).

The pioneering research on PFRP beam-to-column joints (Bank et al. 1990, 1994, Bank and Mosallam 1992, Bass and Mottram 1994, Mottram and Zheng 1996, Smith et al. 1998) used steel-like geometry and bolting connection configurations for simplicity and adaptability but components are of glass fibers and concluded the following (i) failure is initiated by cracking at the web-flange junction of the column sections and the column needs to be strengthened to avoid it; (ii) premature cracking of the cleats connecting the beam and column due to the low fiber content in the direction of loading (non-balanced fiber orientation arrangements). Later the cleats were replaced by steel and stainless-steel ones (Bass and Mottram 1994, Mottram and Zheng 1996, Zhang et al. 2018, Martins et al. 2017, Luo et al 2019, Turvey 2000, Turvey and Cooper 2004, Qureshi and Mottram 2013; Martins et al. 2021a; Qureshi et al 2020; Martins et al. 2021d; Martins et al. 2023), in which the following were observed; (i) premature failure of column's web-flange junction, (ii) local buckling in beam flange; (iii) web and flange cleated joints failed in combination of beam's top flange tensile rupture and shear-out failure in beam webs possibly due to inadequate edge distance (e_2) and end (e_1) distance; (iv) web cleat only joints failed in shear-out of beam web ends possibly due to small end distance (e_1); (v) flange cleat only joints failed in beam's top flange tensile rupture; (vi) the increase in thickness of the steel cleats does not improve the structural performance as the failure mode is always governed by PFRP profiles due to its less stiffness and directionally varying material characteristics; (vii) it is possible to exploit steel yielding before the failure of glass fiber reinforced polymer (GFRP) profiles by strengthening the column and beam with steel components, however, so far this method demonstrated only for tubular sections by placing the steel strengthening components inside the column and beam cross-sections. If a similar strengthening method is used for open cross-sections like I-sections, there will be several individual components and they require more bolted connections which will further complicate the design process. More importantly, in most of the above literature, it was recommended to reinforce the column near the vicinity of the joint to avoid premature web-flange junction failure. Furthermore, manufacturing a complicated shape for uniform load transfer in a PFRP structural joint is uneconomical and the construction is impractical with it. To improve the joint performance and to delay premature failures, new types of connection components were developed (Bank et al. 1994, Mosallam et al. 1994, Smith et al. 1999, Singamsethi et al. 2005), and new connection configurations were also proposed with adhesive bonding (Feng et al. 2022), however, the failure pattern remains brittle. The researchers concluded that the adhesive bonding can improve the strength and achieve the serviceability and stiffness requirements, however, the durability performance of the adhesive connection needs to be investigated with respect to the material characteristics of PFRP and established in the form of design guidelines.

Although research studies on PFRP beam-to-column joints can be found in the literature, the latest comprehensive review work by Coelho and Mottram (2015) and Bank (2023), indicated that the current design specifications (CNR 2008, ASCE 2010) for the PFRP structures are not appropriate to be used by industries and steel alike joints will not be applicable for PFRP structures. Coelho and Mottram (2015) also specified that there is a large research gap in the behavior of the PFRP structural frames, despite the large number of innovations in recent years (Feng et al. 2022), there is a need for new joints configuration to improve the load paths and delay the brittle failure of the PFRP joints. Similarly, the objective of this present investigation is to increase the application of PFRP structures in the corrosive environment and use with sea-sand seawater concrete (Teng et al. 2019) by improving the failure modes and delaying brittle failure. In addition, due to the nature of the PFRP fibers, the bolts and nuts made up of fibers cannot be used in the connections where shear force is influencing the connection stiffness (Abdelkerim 2019 and 2020; Lawler and Polak 2021). Therefore, this study focuses on the development of simple beam-to-column joints made only from PFRP profiles with E-glass fiber except bolts are of stainless steel. The structural behavior of beam-to-column joints is investigated and improved connection element configurations are suggested for better load transfer and delay the first failure. Moreover, the stiffness of the tested joints was determined using the joint component method used for steel joints according to Eurocode (BS EN 1993-1-8:2005) to check its appropriateness, similar design method was adopted by Martins et al. (2021b) for PFRP beam-column joints.

Present Investigation

The PFRP beam-to-column connection element configurations including end distance (e_1), bolt diameters (d_b), bolt spacing (s), and geometric dimensions are designed according to the existing literature (CNR 2008, ASCE 2010, EU 2016, CEN/TS 2020, FprCEN/TS 2022, Martins et al. 2021 and Selvaraj et al. 2023). This research explored the load path and first failure in PFRP beam-to-column joints. The objective of this study endeavors to delay the first failure beyond the serviceability limit load, analyze the load paths-transfer mechanism and determine the contribution of the individual connecting components. The meaning of first failure is the deformation of the connecting element exposing the fibers, followed by a decrease in the stiffness of the joint, and leads to ultimate failure. Thus, the ultimate moment capacity and rotation of the joint are higher than that of the first failure. The first failure in PFRP structures should not be considered as the elastic limit for design calculation, but most of the time it is less than the elastic limit due to the uncertain failure modes of the PFRP materials (Mottram and Zheng 1999a). Further, the appropriateness of the Eurocode (BS EN 1993-1-8:2005) method of stiffness determination is validated by comparing it with the initial stiffness from the experiments.

Material Properties and Specimen Preparation

The PFRP tubular column and I-section beam profiles used in the tests were made from glass fiber products. The material properties and physical characterization of PFRP profiles are obtained from tensile and burn-off tests, respectively. The samples for the tensile and burn-off tests were taken from both flanges and webs of the beam and column. The tensile test samples are of rectangular strip size of 250 mm long and 25 mm wide. The tensile test was conducted according to ASTM D3039/D3039M (2014) and Selvaraj and Madhavan (2020), the material properties obtained from the tensile tests were summarized in Fig. 1 and Table 1. The burn-off tests were carried out according to ASTM D3171 (2015), and Selvaraj and Madhavan (2019). The average fiber weight fraction ratios obtained from burn-off tests were 59.8%, and 56.86% for 4 mm and 9 mm thick PFRP cleat profiles, respectively. The fiber fraction ratios of the PFRP beam (4 mm thick plate profile) and column (5 mm thick plate profile) profiles are 50.56% and 52.73%, respectively. These fiber weight fraction ratios are consistent with the minimum requirements of the standards (CNR 2008, ASCE 2010, EU 2016, CEN/TS 2020, FprCEN/TS 2022). The fiber orientation arrangements (architecture) of all three different thicknesses of PFRP plates (both the web and flanges) are partially balanced symmetric as observed through burn-off tests; there are bi-directional fiber layers on both the top and bottom of the PFRP plate and one bi-directional fiber layer on the mid-thickness but thinner than the top and bottom layers; other fibers are unidirectionally oriented in the longitudinal directional of the member as shown in Fig. 1a.

The column is of a square tubular profile 100 mm × 100 mm (outer-to-outer dimensions) with a wall thickness of 5 mm and the beam is of I-section of size 100 mm deep, 80 mm flange width, and thickness of 4 mm for both flange and web (Fig. 2a). The column is filled with C25 grade concrete (25 MPa - characteristic compressive cube strength) as shown in Fig. 2b as a strengthening measure to avoid web-flange junction failure. The concrete mix of 1:1:2 is used to achieve the 25 MPa strength, meaning 554 kg of cement per cubic meter of concrete. It was anticipated based on the literature that the connection components would fail first if the column is strong, therefore, the concrete strength is arbitrarily chosen. The objective of this investigation is to analyze the failure modes of the connection components, therefore the column and beam dimensions are consistent for all the test samples, while the size of the connecting components (flange and web cleats) and connection geometries (stiffened, unstiffened cleats and joints with T-stiffener) are varied as summarized in Table 2 and Figs. 2f-2o.

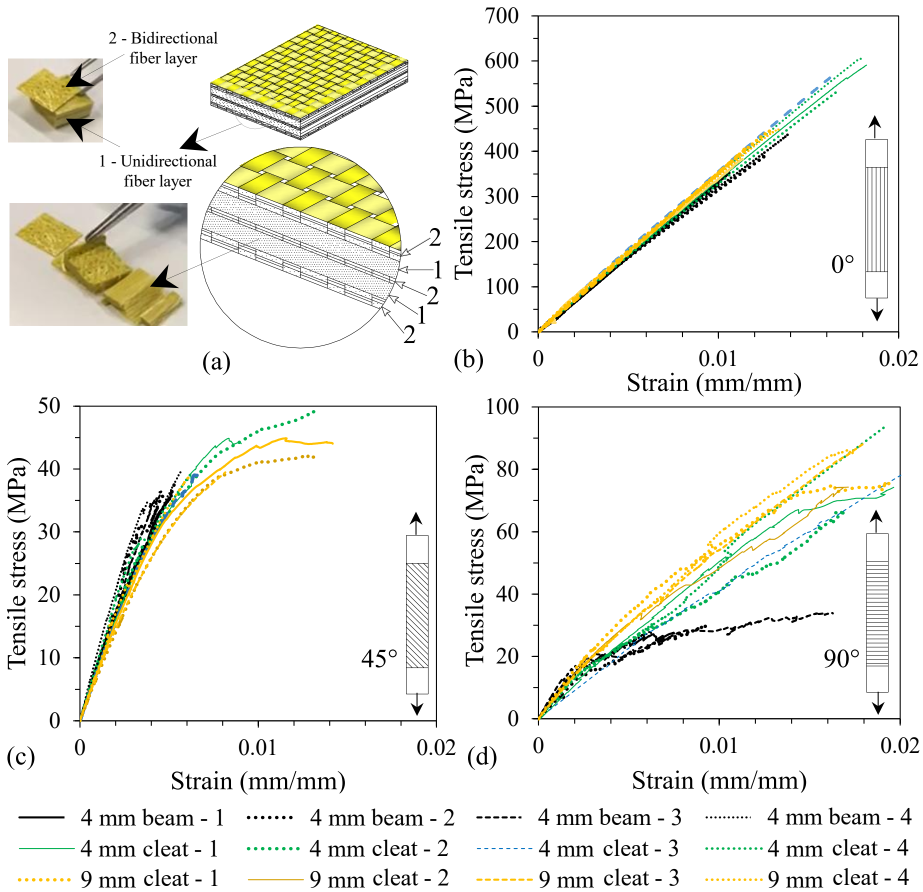

Fig. 1. Material and physical characteristics of PFRP structural sections: (a) Fiber architecture of the PFRP plates observed from burn-off tests; (b) Stress-strain curve of PFRP plates tested at 0-degree loading angle; (c) Stress-strain curve of PFRP plates tested at 45-degree loading angle; (d) Stress-strain curve of PFRP plates tested at 90-degree loading angle;

Table 1. Material properties of the PFRP structural shapes tested

Thickness of the PFRP	Sample number	Tensile Modulus (E) (MPa)[a]			Ultimate Strain (ε) %[a]			Ultimate Tensile Strength (f_t) (MPa)[a]		
		$E_{t,L}$ [0°]	$E_{t,D}$ [45°]	$E_{t,T}$ [90°]	0°	45°	90°	0°	45°	90°
4 mm (beam's flange and web)[1, b]	1	32782	7266	6879	1.82	0.74	1.44	590.9	36.1	49.8
	2	32053	6991	5719	1.66	0.81	1.19	532.6	35.9	50.7
	3	34639	7150	6884	1.62	0.57	1.49	562.8	34.3	55.0
	4	33870	8331	6031	1.79	0.54	1.05	605.8	35.5	51.3
Mean		33336	7435	6378	1.72	0.67	1.29	573.0	35.4	51.7
COV		0.03	0.08	0.09	0.06	0.20	0.16	0.06	0.02	0.04

4 mm (cleats)[2]	1	33516	8507	7640	1.06	0.50	0.75	352.0	35.3	27.6
	2	31031	8650	5929	1.27	0.53	0.93	394.5	37.6	29.8
	3	32877	8626	8672	1.01	0.46	1.51	330.0	36.8	33.9
	4	31539	10113	6548	1.38	0.57	0.62	436.8	39.5	27.8
Mean		32241	8974	7197	1.18	0.51	0.95	378.3	37.3	29.8
COV		0.04	0.08	0.17	0.15	0.09	0.41	0.12	0.05	0.10
9 mm (cleats)[3]	1	34705	7640	7646	1.29	1.15	2.46	445.0	44.9	83.0
	2	33535	6886	6780	1.13	1.28	1.71	382.2	42.1	82.8
	3	35293	7264	6625	1.15	0.82	1.80	404.1	39.5	88.4
	4	34141	8401	6855	1.34	0.62	1.71	448.4	39.3	86.1
Mean		34419	7548	6977	1.23	0.97	1.92	419.9	41.4	85.1
COV		0.02	0.09	0.07	0.08	0.31	0.19	0.08	0.06	0.03

[a]Test results E, ε, and f_t are summarized with respect to the corresponding angle of loading; [b]average values of the beam's flange and web - the difference was insignificant as the thickness and fiber architecture were same in both flange and web; [1] the results were calculated from the stress-strain plots with legends "4 mm beam - 1" to "4 mm beam - 4" in Figs. 1b -1d; [2] the results were calculated from the stress-strain plots with legends "4 mm cleat - 1" to "4 mm cleat - 4" in Figs. 1b -1d; [3] the results were calculated from the stress-strain plots with legends "9 mm cleat - 1" to "9 mm cleat - 4" in Figs. 1b -1d.

Table 2: Dimension of the test samples and corresponding test results.

Specimen Nomenclature	Flange and web cleat thickness (mm)	e_1 (mm)	Stiffened or unstiffened cleats	Ultimate moment (kNm)	Initial Stiffness (kNm/rad)
T4 - 4e1 - L - Fig. 2f	4	$4d_b = 24$	Unstiffened	4.61	48.48
T4 - 6e1 - L - Fig. 2g	4	$6d_b = 36$	Unstiffened	5.45	51.52
T4 - 8e1 - UL - Fig. 2h	4	$8d_b = 48$	Unstiffened	5.08	47.88
T4 - 8e1 - L - Fig. 2i	4	$8d_b = 48$	Unstiffened	6.21	54.64
T9 - 4e1 - L - Fig. 2j	9	$4d_b = 32$	Unstiffened	4.80	56.62
T9 - 6e1 - L - Fig. 2k	9	$6d_b = 48$	Unstiffened	6.77	68.35
T9 - 8e1 - UL - Fig. 2l	9	$8d_b = 64$	Unstiffened	6.87	131.50
T9 - 8e1 - L - Fig. 2m	9	$8d_b = 64$	Unstiffened	7.24	139.92
T4 - 4e1 - UL - T - Fig. 2n	4	$4d_b = 24$	T-Stiffener	5.55	146.57
T4 - 8e1 - UL - T - Fig. 2o	4	$8d_b = 48$	T-Stiffener	6.43	161.93

Note: e_1 - end distance; d_b - diameter of the bolt; $e_2 \geq 2d_b$ for all the connections tested. The nomenclature of the specimens are as follows - Thickness of the cleats - end distance (with respect to the diameter of the bolts - d_b) - L for stiffened cleat and UL for unstiffened cleat - T for T-stiffeners on both the flanges, for example, T4 - 4e1 - L means 4 mm thick flange and web cleats with $4d_b$ end distance and stiffened cleat; and T4 - 4e1 - UL - T means 4 mm thick flange and web cleats with $4d_b$ end distance and unstiffened cleat with T-stiffeners. Please refer to Table 1 for the material properties of the structural members used.

The length of the column and beam is 1360 mm and 900 mm, respectively as shown in Fig. 2e. The beam is connected at a distance of 550 mm from the top of the column. Since the column is of tubular sections, the bolts are connected through the column cross-section. It is also a strengthening measure to use the through bolts to avoid web-flange junction failure. The stainless-steel bolts with Young's modulus 194 GPa were used for all connections, and they were pre-tightened on the column before casting the concrete as shown in Fig. 2b.

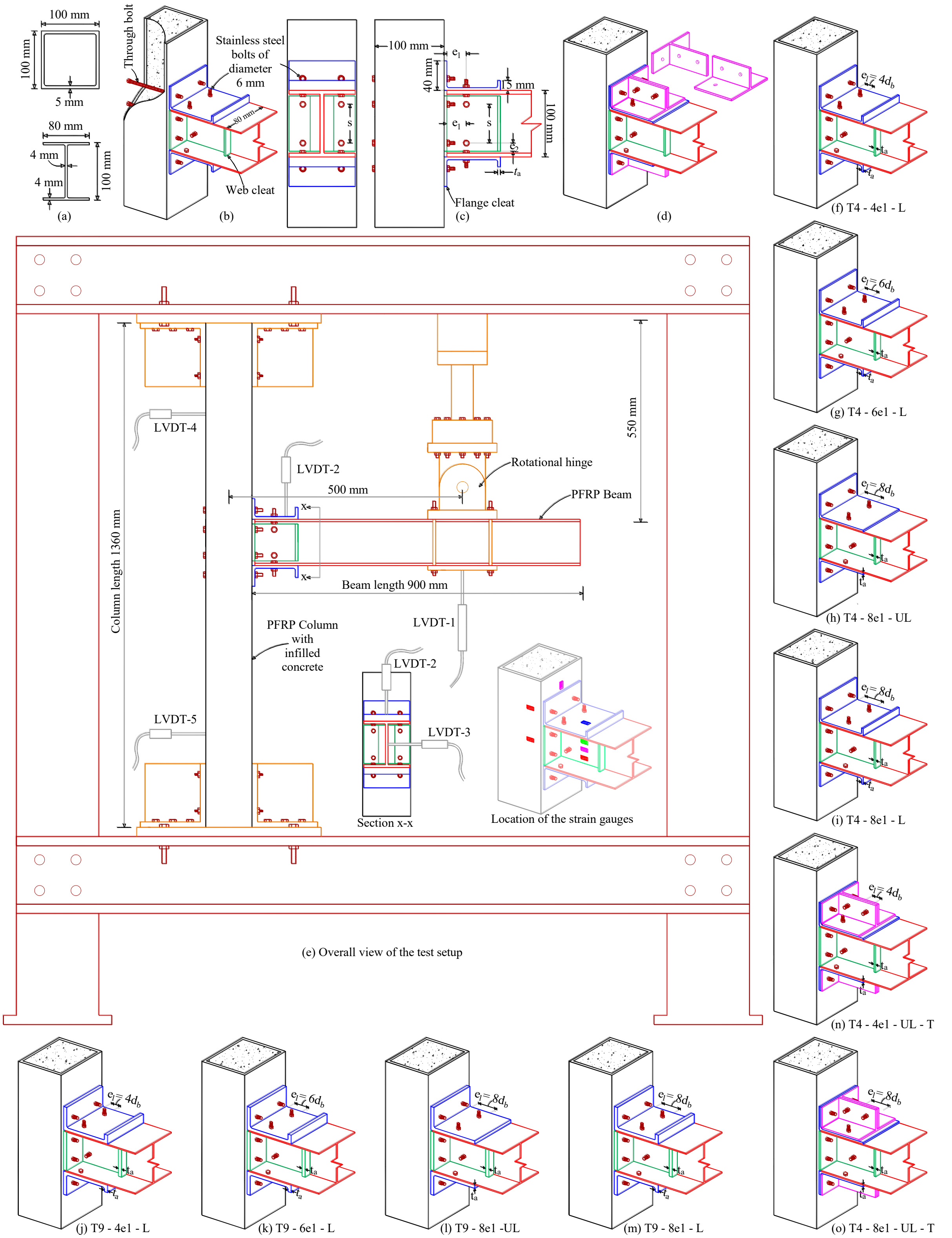

Fig. 2. PFRP Beam-to-column joint specimens and testing arrangements: (a) Dimensions of the column (Square tubular section) and beam (I-Section); (b-c) Design dimensions and connection arrangements; (d) Connection with T-Stiffener; (e) Test set-up for beam-to-column joint; (f-o) View of the specimens with varying parameters

All the bolts used for the beam-to-column joints were 6 mm in diameter as per CEN/TS (2020), which suggests that the diameter of the bolts should be equal or 1.5 times the thickness (t_a) of the PFRP plate that is connected ($t_a \leq d_b \leq 1.5t_a$). The two-bolted and one-row connection was employed at each connecting component as shown in Fig. 2c and 2d. The beam and column are connected using flange and web cleats which were cut from unequal angle sections, therefore the direction of fibers in the web and flange cleats are perpendicular to the longitudinal fibers of the beam as shown in Fig. 3. The T-shape stiffener is introduced with both top and bottom flange cleats for verifying the increase in stiffness and moment capacity of the beam-to-column joint (Fig. 2d, 2n and 2o). The T-stiffeners are cut from the PFRP I-section profile by removing one flange, therefore, the fiber architecture remains consistent with other components of the joint. The details of connection dimensions for each tested specimen are summarised in Table 2.

Test Setup

The beam-to-column tests were performed in a steel loading frame. The concrete-infilled PFRP column ends were connected firmly to the frame. The column was fixed at both ends to resist the rotations due to the loading on the beam, therefore the load transfer ability of the connecting components can be analyzed. The loading was applied using a hydraulic jack with a capacity of 250 kN. A rotational hinge was used at the loading point to keep the load perpendicular to the beam alignment. The loading was applied by a monotonic deflection, the load cell reaction was obtained as a load. The deflection was applied on the beam at a distance of 500 mm from the center line of the column. The rate of loading is such that the ultimate failure of the PFRP joint occurred within 20 minutes of loading. A total of five linear variable displacement transducers (LVDTs) were positioned to measure the displacement profile of the beam-to-column joint as shown in Fig. 2e. The strain gauges were instrumented on the beam, column, and connecting cleats to measure the strain corresponding to the applied load (Figs. 2e). The inclinometer was positioned at the end of the beam to measure the rotation. The data from loadcell, LDVTs, strain gauges, and inclinometer were gathered by a data logger. The actual photos of the test arrangement before loading and after failure are shown in Fig. 4.

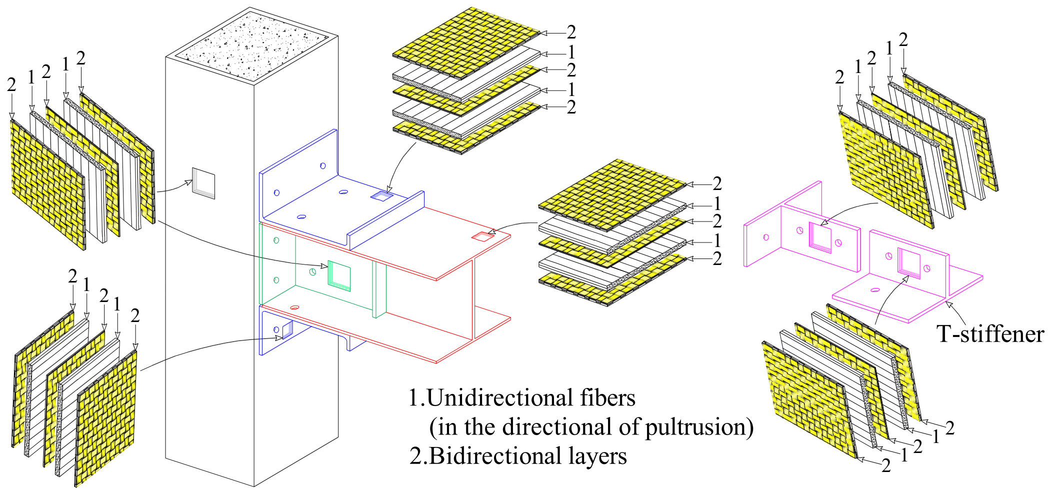

Fig. 3. Alignment of connection components fiber orientations in the beam-to-column joint

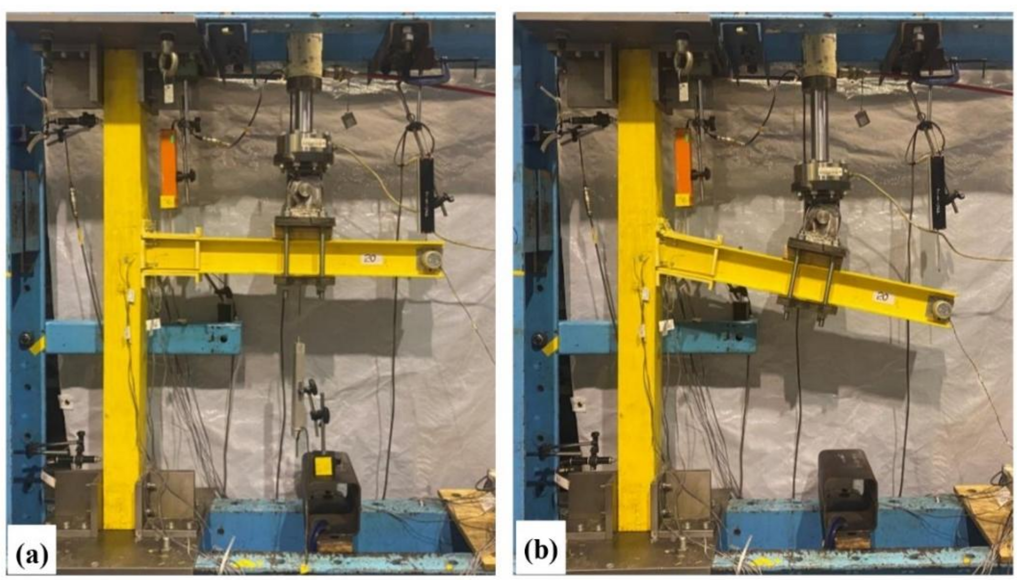

Fig. 4. Actual photo of the beam-to-column joint test arrangements: (a) Photo before the test; (b) Photo of the tested sample

Results and Discussion

General observation

In general, all the tested beam-to-column joint configurations exhibited brittle failure due to cleats corner cracking and rupture of the stiffener, however, the increase in initial stiffness and moment capacity was observed with an increase in the thickness of the cleats and end distance (e_1). The ultimate moment capacity and initial stiffness of the joints are summarized in Table 2 and Figs. 5-9. Overall, it was observed that the top flange clip failed first followed by the failure of the web cleats in all the tested samples, and the use of T-stiffeners delayed the first failure to some extent. The strain readings from the connection components (Figs. 2e, 6a, and 7a) are used for a detailed understanding of the failure mode, contribution, and load transfer between the connection components. As the PFRP beam-to-column joint's structural response varied depending on the different components, the joint behavior is analyzed with respect to individual parameters in the following sections.

Effect of end distance (e_1)

The end distance (e_1) is one of the important parameters that govern the failure mode of the PFRP joints, the design codes (CNR 2008, ASCE 2010, EU 2016) suggest that the minimum end distance (e_1) of $4d_b$ should be sufficient, but the latest research (Martins et al. 2021 and Selvaraj et al. 2023) reported that the minimum end distance should be equal to $8d_b$ for attaining the progressive bearing failure. Therefore, to determine the suitable end distance (e_1) for a full-scale joint design application, the end distance is varied from $4d_b$ (minimum limit specified in the codes) to $8d_b$ (minimum limit specified by latest research). In addition, the new design parameter proposed by Selvaraj et al. (2023), covering plate slenderness and end distance $(w/t) / (e_1/d_b) \geq 1.5$ is also followed. Overall, three different end distances (e_1) are varied to check their influence ($4d_b$, $6d_b$, and $8d_b$) (Table 2). The variance in the end distances is configured in all the connecting components like flange cleat, web cleat, and beam for consistency and alignment (Figs. 2c, 2f-2o).

The influence of end distance is significant in the structural response of the beam-to-column joints, as the moment capacity (in kNm) and initial stiffness (in kNm / rad) are significantly increased with an increase in end distance (e_1) as can be observed in Fig. 5a (results of 4 mm cleats), 5b (results of 9 mm cleats), 5c (stiffness comparison), 5e (moment comparison) and Table 2. Compared to the smaller end distance of $4d_b$, the specimens with longer end distances withstand 18.3% and 34.7% higher moment capacity for $6d_b$ and $8d_b$ end distances, respectively, in 4 mm thick cleats (compare T4 - 4e1 - L with T4 - 6e1 - L and T4 - 8e1 - L in Fig. 5e and Table 2), whereas in 9 mm thick cleats, the moment increment is 41.2% and 50.9% for $6d_b$ and $8d_b$ end distances, respectively compared to $4d_b$ end distance (compare T9 - 4e1 - L with T9 - 6e1 - L and T9 - 8e1 - L in Fig. 5e and Table 2). This should be attributed to the fact that the connection closer to the column face [with smaller end distance ($e_1 = 4d_b$) T4 - 4e1 - L] distributes the load within a smaller area ($4d_b$ x thickness of flange cleat) which resulted in higher stress and led to cracking along the entire width of the top flange cleat at the fillet radius location. Whereas in the flange cleats with longer end distance [($e_1 = 8d_b$) T4 - 8e1 - L], the cracking is delayed due to less concentric stress of a corresponding load. However, the cracking of the top flange cleat is the first failure in all the tested samples as marked in Figs. 6j-6q (see strain readings of the flange cleats). It should be noted that there was no visible deformation in the vicinity of the bolt holes (no bearing deformation) in the beams with respect to the change in end distance (e_1) [as shown in Figs. 6b-6i (bolt holes connecting web cleats) and Figs. 7c-7i (bolt holes connecting flange cleats)], this may be due to the connecting components failing well within the elastic limit (first top flange cleat failure).

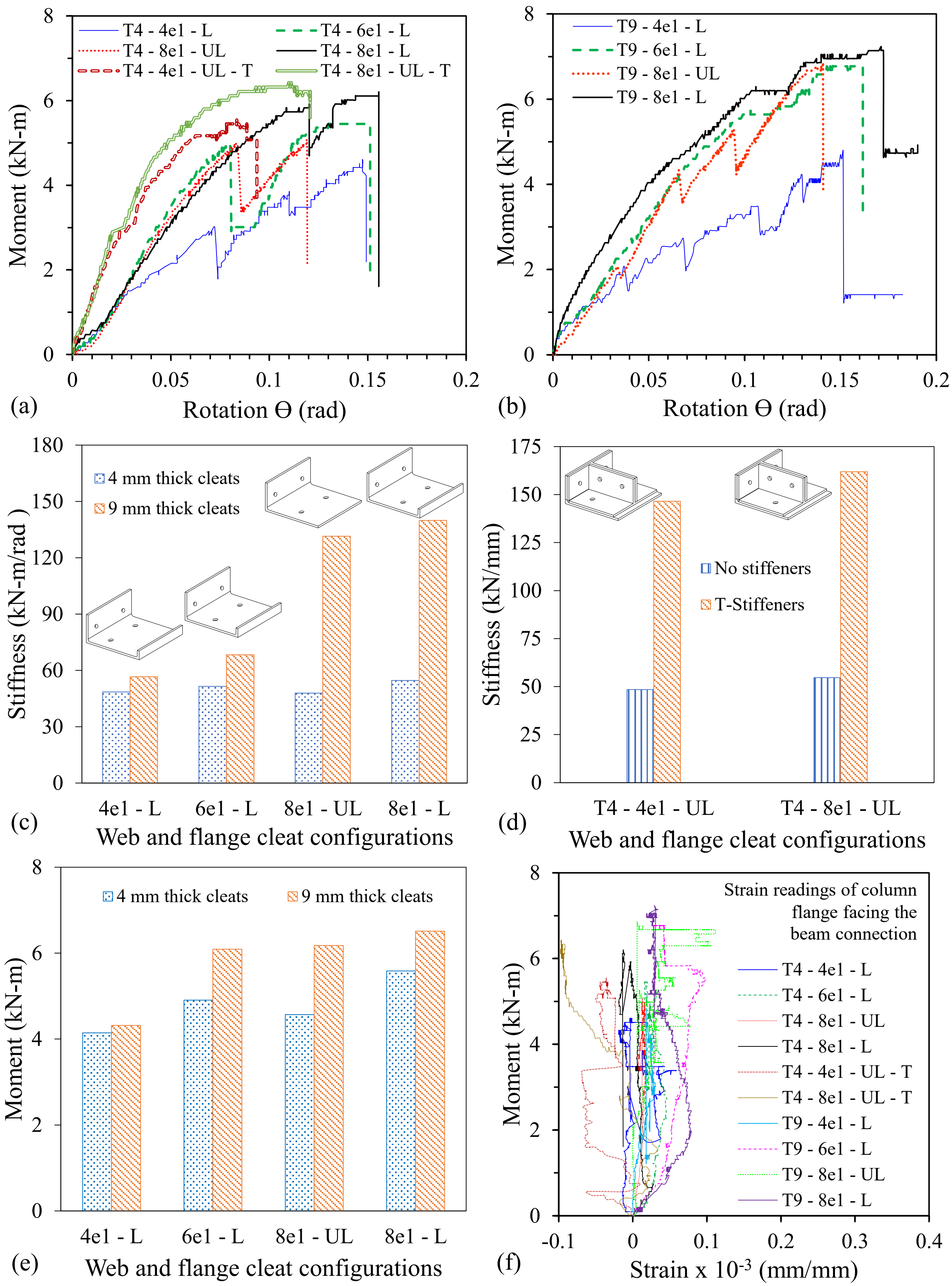

Fig. 5. Test results of PFRP beam-to-column joints: (a) Moment-rotation plot for 4 mm thick cleats and connections with T-Stiffeners; (b) Moment-rotation plot for 9 mm thick cleats; (c-e) Variation in stiffness and ultimate moment with respect to the different geometry parameters of the connection components; (f) Strain readings of column flange facing the beam connection.

The influence of end distance (e_1) was not observed in the initial stiffness (within 40% of the loading) of the 4 mm thick flange and web cleat specimens due to less area for load transfer and the stiffness of the connections (T4 series) with varying end distances are between 47.9 kNmm/rad to 54.6 kNmm/rad as shown in Fig. 5c and Table 2. Whereas, in the case of specimens with 9 mm thick flange and web cleats, the initial stiffness for the end distance of $8d_b$ increased by 147.1% and 104.7% compared to $4d_b$ and $6d_b$ end distances, respectively as shown in Fig. 5c and Table 2. This increase in initial stiffness only found in the $8d_b$ end distance in 9 mm thick connection components may be attributed to the combined influence of a higher area of loading and more free length to elongate (longer end distance × cleat thickness) and the presence of thick bidirectional layers of fibers in the 9 mm thick flange and web cleats. It should also be noted that the influence of e_1 was observed only in 9 mm thick cleated connections and not in 4 mm thick cleated connections, this should be due to the fact that the higher area of loading in 9 mm cleats with longer free length ($6d_b$ and $8d_b$) to elongate taken more load prior to first crack. Though the bidirectional layer in 9 mm cleats provides resistance against rotation at the initial stage (stiffness), the improvement in moment capacity is insignificant (4.1 to 35.3%) compared to 4 mm cleats as shown in Fig. 5e (compare 4 mm thick cleat specimens and corresponding 9 mm thick cleat specimens). Based on the above observations, it is clear that the increase in cleat thickness with adequate end distance (e_1) would improve the behavior of the PFRP beam-to-column joints.

Failure of flange and web cleats

As mentioned previously, the flange and web cleats were cut from the PFRP unequal angle profiles, therefore the longitudinal fibers of the cleats were aligned perpendicular to the beam's longitudinal fibers as shown in Fig. 3. However, it should be noted that all the PFRP profiles used in this study are of partially balanced symmetric (three layers of bidirectional layers with longitudinal fibers) as shown in Fig. 1a. This perpendicular alignment of the cleat's longitudinal fibers significantly influenced the overall failure mode of the beam-to-column joints owing to the nature of the PFRP' structural behavior. In general, the PFRP profiles have less resistance in the lateral or through-thickness direction compared to the longitudinal direction (Mottram and Zheng 1999a; 1999b and Selvaraj et al. 2023). In comparison, both the flange and web cleats failed prematurely at the fillet corner radius irrespective of the thickness, nevertheless, the increase in moment capacity and initial stiffness of the joint is observed as shown in the moment versus displacement plots in Figs. 5a (4 mm thick cleats) and 5b (9 mm thick cleats). The initial stiffness of the beam-to-column joint increased by 156.1% and 174.6% in specimens with an end distance of $8d_b$ in 9 mm thick cleats compared to the corresponding 4 mm thick cleats as shown in Fig. 5c, but for specimens with an end distance of $4d_b$ and $6d_b$, the stiffness increment is insignificant (16.8-32.7% only). In addition, the increment in moment capacity is also not significant, to be precise, the flange and web cleat thicknesses more than doubled from 4 mm to 9 mm [compare 4 mm thick cleats and corresponding 9 mm thick cleats in Figs. 5c (stiffness comparison) and Fig. 5e (moment comparison)] but the improvement in moment capacity is only about 4.1 to 35.3% as shown in Table 2. In structural design when the cross-sectional area of the member is doubled the stiffness and loading capacity should also be doubled or proportionally increased, however in the present study due to the natural behavior of PFRP profiles the moment and stiffness did not improve proportionally for all the specimens. The significant increase of stiffness in 9 mm thick cleats compared to corresponding 4 mm thick cleats with an end distance of $8d_b$ indicates that the end distance (e_1) also plays a role in stiffness improvement.

The top flange cleat which was in the tension zone of the joint configuration failed first due to cracking at the fillet corner radius in all the tested samples, as shown in Figs. 6b-6i, and Fig. 8b.

It is important to note that the failure of the top flange cleat occurred at the small deflection (Figs. 6j to 6q - see the top flange strain values), leading to progressive stiffness reduction in the joint (Figs. 5a and 5b), however, the overall joint was still within the elastic limit (the strain values corresponding to the first failure in the top flange is less than the elastic strain), or in other words the first failure occurred well within the elastic strain limit. The bottom flange cleat which was in the compression zone of the joint did not fail or crack till the end, it avoided the sudden/brittle failure, or in other words delayed the overall failure of the joint, as observed from the linear compression strain reading in Figs. 6j-6q (see the bottom flange strain values). This should be attributed to the fact that the bottom flange cleats were in a compression zone and its deformation was well controlled by the column face to which it was connected as indicated in Fig. 6a. Theoretically, the overall joint stiffness is significantly influenced by the effectiveness of the column flange to which the cleats are connected (Martins et al. 2021b). If the column rotates with respect to the beam's rotation, then the stiffness will decrease drastically. In the present investigation, the column was infilled with concrete, and the bolts connecting the flange and web cleats were through the entire column width (Fig. 2b), therefore there was no failure at the fillet radius of the columns (web-flange junctions) and there was no rotation or displacement at the column ends, as a result, the column stiffness was high and it provides adequate stability against the compressive force from the bottom flange cleat as shown in Figs. 8b-8e. The comparison of strain readings of the column flange facing the beam connection (Fig. 5f) and other stain readings (Figs. 6j-6q, Fig. 7b, and Fig. 8a), shows that the column was well within the elastic range yet the failure was completely influenced by the premature failure of the connecting components. The web cleats failed in cracking due to the rotation of the beam (pulling force on the top portion), and notably, the crack in the web cleat was initiated only after the top flange failure.

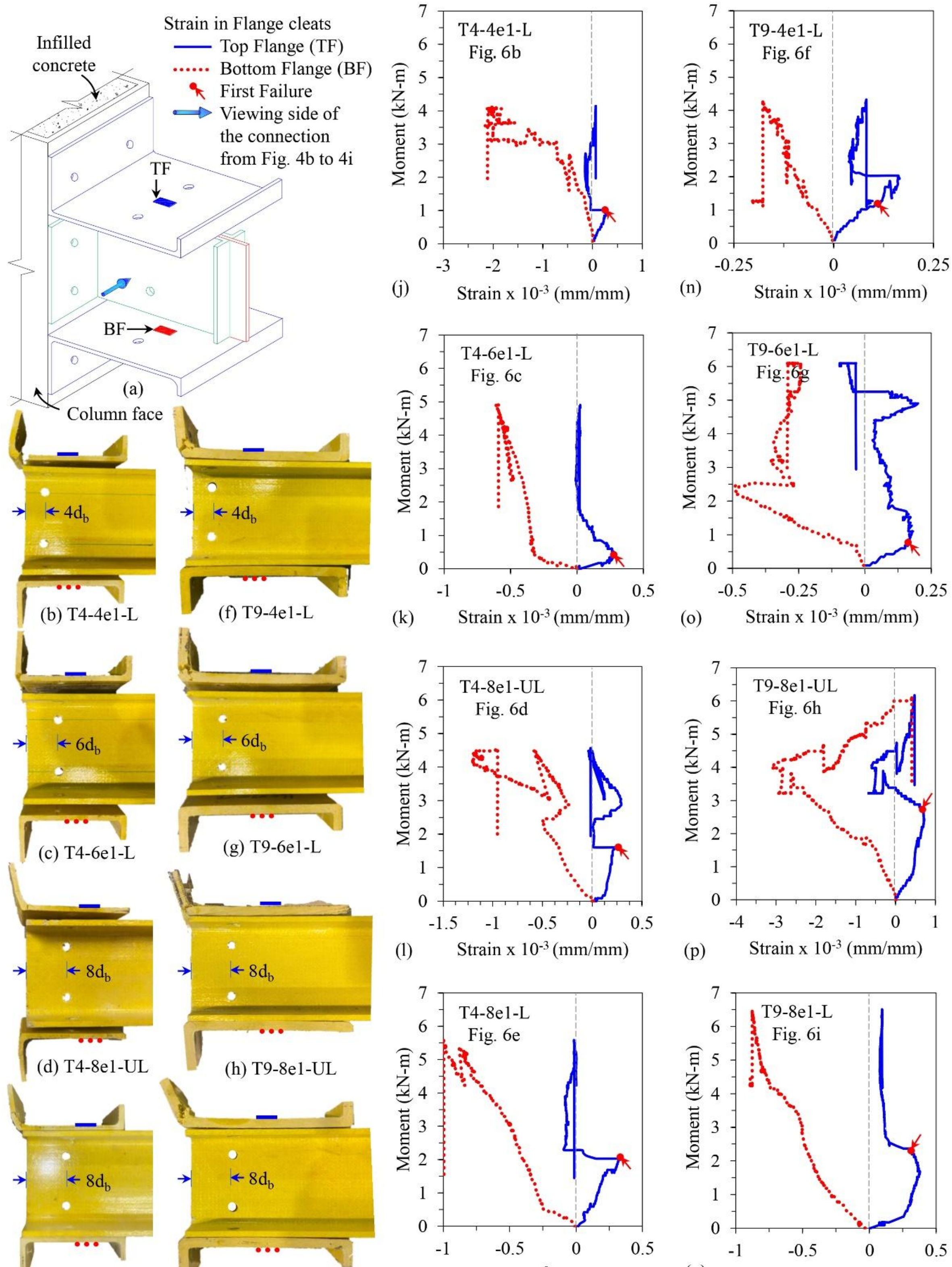

Fig. 6. Failure mode of the flange cleats and corresponding strain readings: (a) Location of the strain gauges in flange cleats; (b-i) Failure mode of flange cleats and deformation in beam's web portion bolt holes; (j-q) Top and bottom flange cleat strain readings

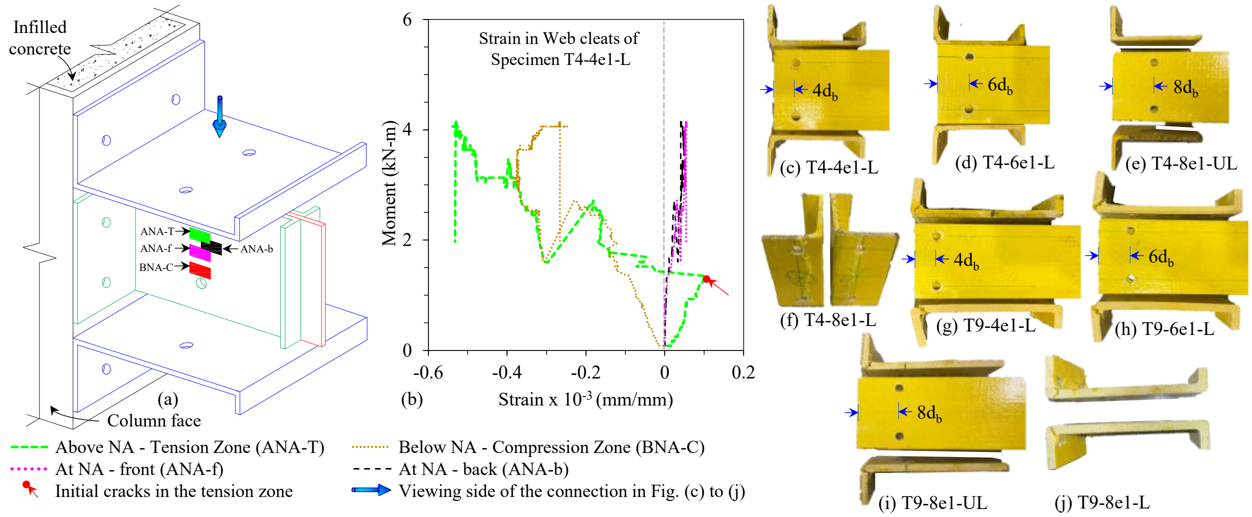

Fig. 7. Failure mode of the web cleats and corresponding strain reading (sample reading specimen T4-4e1-L only): (a) Location of the strain gauges in web; (b) Web cleat strain readings; (c-i) Failure mode of web cleats and deformation in beam's flange portion bolt holes;

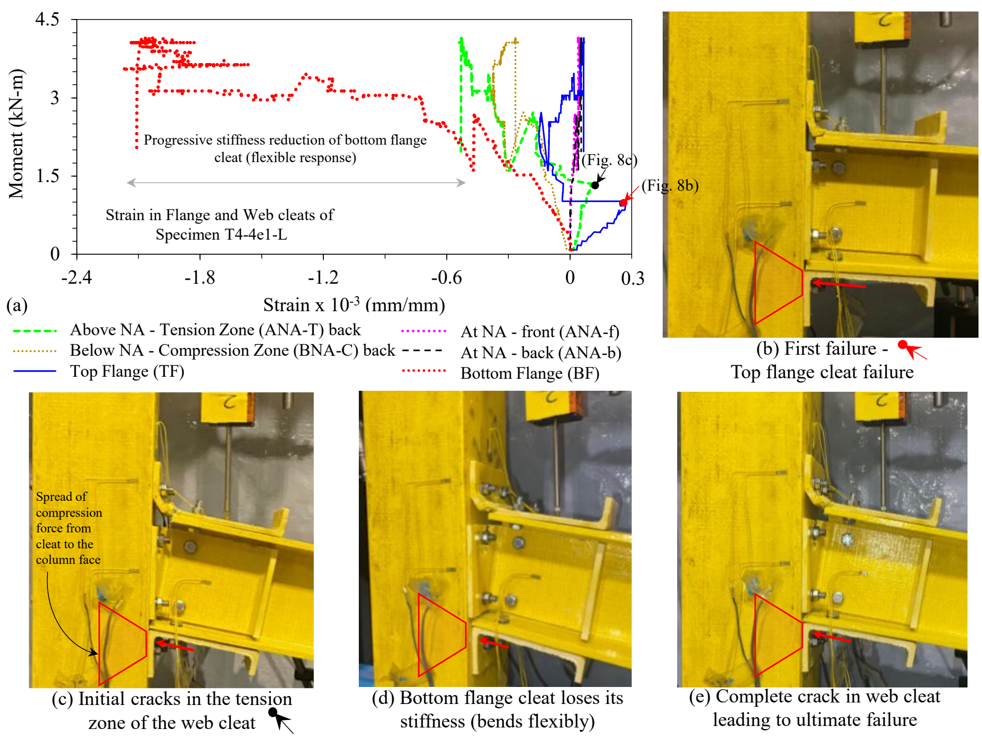

Fig. 8. Failure mode pattern in PFRP beam-to-column connections without T-stiffeners: (a) Strain in the flange and web cleats of specimen T4-4e1-L; (b-e) Initial to ultimate subsequent failure modes

This can be observed from the moment vs. strain plot in Fig. 8a, first the top flange strain readings suddenly changed to zero due to cracking (red arrow in Fig. 8a and corresponding first failure mode Fig. 8b), later, the strain reading of the web cleat [curve with the legend "Above NA -

Tension Zone (back)" in Fig. 8a] also exhibited sudden change from gradual increase due to cracking (corresponding failure mode is shown in Fig. 8c). After the occurrence of first crack in web cleat, the strain readings were not accurate and shown random pattern due to the drop-in stiffness, thus strain reading after crack can be ignored. The failure pattern of the beam-to-column joint configuration investigated in the present study is, (i) first top flange cleat failure; (ii) followed by initial cracks in the web cleat and (iii) bending of the bottom flange cleat (flexible response - bending without resistance), finally (iv) complete crack in web cleat at the fillet radius location leading to ultimate failure. The above-mentioned failure mode pattern is depicted in Figs. 8b to 8e, the same pattern can be observed at the moment vs. displacement plots (Figs. 5a and 5b) through the following stages: (i) linear elastic until the first failure; (ii) progressive stiffness reduction after the first failure; (iii) further significant stiffness reduction after web cleat crack; and (iv) sudden load drop due to complete crack in web cleat. A slight variation to the above moment vs. displacement plot pattern was observed in some specimens with 4 mm thick cleats (T4 - 4e1 - L, T4 - 6e1 - L, and T4 - 8e1 - UL) in Fig. 5a, this should be attributed to the combined effect of inadequate cleat thickness, small end distance and/or unstiffened cleats. The overall observation indicated that the first failure is well within the service load limit (see Table 3) [which is 40% of the ultimate moment in general (Uy et al. 2017)], therefore it is necessary to delay the first failure by adding more load transfer connection components. Moreover, based on the above observations pertaining to the failure modes in PFRP beam-to-column joint, the following specific conclusion can be made (i) the increase in thickness of the connecting components (flange and web cleats) does not improve the connection behavior proportionally, (ii) the thicker PFRP profiles like 9 mm cleat angles should have adequate end distance (e_1) and more bidirectional layers to avoid sudden cracking; (iii) more load transfer connecting element is required for delaying the brittle failure (improve the initial stiffness).

Contribution of Connection Components

Before understanding the need for additional load transfer connecting elements, it is necessary to comprehend the contribution of each connection component including, top flange cleats, web cleats, and bottom flange cleats in the unstiffened connection configurations. However, it is complicated to determine the contribution of each connection component at each stage of loading due to the complex failure modes of PFRP profiles, nevertheless naturally if one component fails then the other components share the load until overall failure, based on this approach, the strain readings can be used to determine the stage at which each component failed and how others contribute to the load transfer (Table 3). At the initial stage of the loading, all the connection components take the load sharing, therefore the moment versus deflection plot exhibits a linear elastic pattern. The first failure occurred in the range of 10% to 30% and 39% of the ultimate moment (which is within the serviceability limits) in specimens with 4 mm and 9 mm thick cleats, respectively, as shown in Figs. 5a-5b, and Figs. 6j-6q, Fig. 7b and Fig. 8a, (see strain readings of flange cleats) and Table 3. After that, the stiffness of the overall joint started reducing progressively, and the initial cracks in the tension zone of the web cleat occurred at an average of 46% of the ultimate moment which is an average of 15% higher moment than the first failure (top flange failure). Once the web cleat began to crack, the stiffness of the joint dropped drastically, and then the joint resisted the load with the help of the stiffness provided by the bottom flange cleat, which also became flexible as the crack propagated in the web cleat due to rotation. Finally, the web cleats fully cracked at an average of 75% to 82% of the moment capacity. The above interpretation indicates that the first failure caused the subsequent failure modes, therefore an additional connection component is required to delay the first failure.

Table 3: Contribution of the connection components.

Specimen Nomenclature	Initial Stiffness (kNm/rad)	Ultimate moment (kNm)	Moment at First failure (kNm) *	Moment at initial crack in web cleat (kNm) *	Moment at full crack in web cleat (kNm) *
T4 - 4e1 - L	48.48	4.61	1.00	1.30	2.70
T4 - 6e1 - L	51.52	5.45	0.50	2.00	4.50
T4 - 8e1 - UL	47.88	5.08	1.50	2.50	4.50
T4 - 8e1 - L	54.64	6.21	2.00	3.10	5.20
T9 - 4e1 - L	56.62	4.80	1.10	1.28	2.45
T9 - 6e1 - L	68.35	6.77	0.75	2.43	5.10
T9 - 8e1 - UL	131.50	6.87	2.65	3.20	4.75
T9 - 8e1 - L	139.92	7.24	2.30	3.45	5.60
T4 - 4e1 - UL - T	146.57	5.55	2.75	3.20	4.65
T4 - 8e1 - UL - T	161.93	6.43	2.90	3.15	4.90

Note: * The moment values at the particular failure modes are observed based on the strain gauge readings as shown in Figs. 6-9.

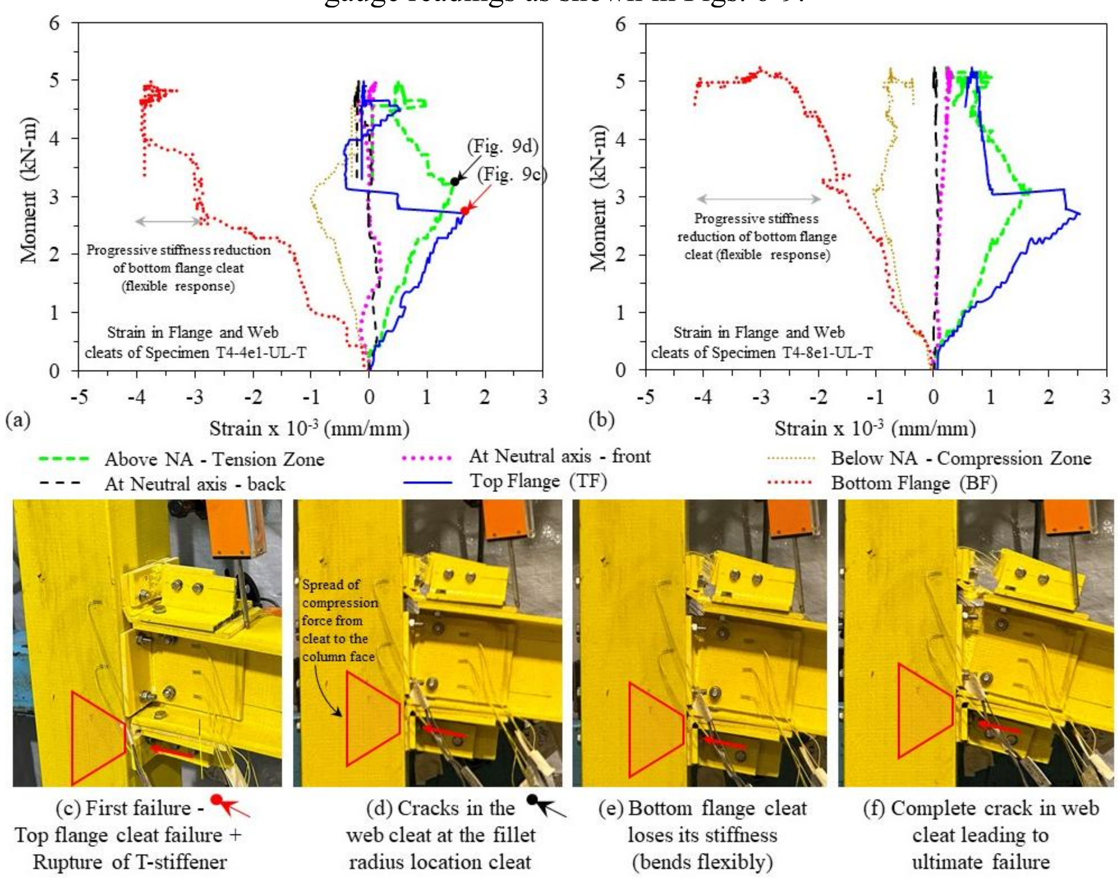

Fig. 9. Failure mode pattern in PFRP beam-to-column connections with T-stiffeners: (a) Strain in the flange and web cleats of specimen T4 - 4e1 - UL - T; (b) Strain in the flange and web cleats of specimen T4 - 8e1 - UL - T; (c-f) Initial to ultimate subsequent failure modes

A T-shape stiffener was added in both the top and bottom flange, one T-stiffener was connected from the column face side, and another T-stiffener was connected from the beams flange side, and both of them joined at the convergence point using two bolts as shown in Fig. 2d. Addition of T-stiffeners is a simple method to increase the load share of the flanges, and they take part in both top and bottom flange load share simultaneously, therefore, the initial stiffness increases significantly. The T-stiffeners are 4 mm thick and they are added to 4 mm thick flange cleat connections, T4-4e1-UL-T (Fig. 2n) and T4-8e1-UL-T (Fig. 2o). In the top flange, the T stiffeners are under tension due to the pulling force of the beam to the column, simultaneously, at the bottom flange the T-stiffeners provide stiffness against the bending (T-stiffeners transfers compression force from one leg of the bottom flange cleat to the other leg that is connected to the column face). Owing to this load transfer pattern, the stiffness of the joint was increased significantly as shown in Fig. 5a and Fig. 5d. More importantly, the first failure was delayed up to 2.75 kNm moment in T4-4e1-UL-T specimen (see in Fig. 9a and Table 3) which is 175% more than the occurrence of first failure in similar specimen without stiffener T4-4e1-L (see in Fig. 8a and 6j). Similarly, in specimen T4-8e1-UL-T the first failure occurred at a moment value of 2.9 kNm (Table 3) which is 93.3% higher than the corresponding specimen (T4-8e1-UL) without stiffeners where the first failure occurred at 1.5 kNm moment (Fig. 6l). But once the top flange T-stiffener failed together with top flange cleat cracking (Fig. 9c), the joint loses its stiffness and the progressive stiffness reduction began. This indicates that the provision of an additional load transfer component in the form of a T-stiffener can improve the stiffness significantly and delay the first failure. This delayed failure can help in achieving the serviceability limit before the first failure which is an important design specification for PFRP structures design (Mottram 1994, Mottram 1996, Mottram and Zheng 1996 and 1999a). It should be noted that the moment capacity did not increase significantly after adding the T-stiffeners (Fig. 5a). However, a significant improvement in stiffness was achieved and the first failure was delayed beyond 45% of the ultimate moment (which is higher than the service load) by adding a T-stiffener to the 4 mm thick cleats, perhaps if the T-stiffeners were added to 9 mm thick cleats, the moment capacity could have been improved. Moreover, the thickness of the T-stiffener can also be increased based on the need. It is important to note that due to the manufacturing procedure, the fibers in the T-stiffeners are perpendicular to the tensile force as shown in Fig. 3, therefore the T-stiffeners failed in rupture (Figs. 9d-9f), this failure mode can also be improved by increasing the number of bidirectional fiber layers in the PFRP fiber architecture (use of more balanced symmetric architecture than partially balanced symmetric). Further, adhesive bonding can also be introduced for the connection between connecting components and members to delay the first failure mode, however, the long-term durability performance should be assessed experimentally.

Determinization of Stiffness of the PFRP beam-to-column joint

The establishment of design standards is an essential task for promoting any structural materials. PFRP is one of the structural materials that has a variety of material specifications including their anisotropy, inhomogeneity and various industries have different norms, therefore, it is essential to develop internationally acceptable design standards (Bank et al. 2023; Coelho and Mottram 2015). The present study suggests the design method to determine the initial stiffness of the PFRP beam-to-column joint after checking the appropriateness of the joint component method from Eurocode (BS EN 1993-1-8:2005). This design method was used by Martins et al. (2021b) for flange-cleated beam-to-column connections, however, in the present study the Eurocode method is modified according to the connection configuration, load transfer, and failure modes.

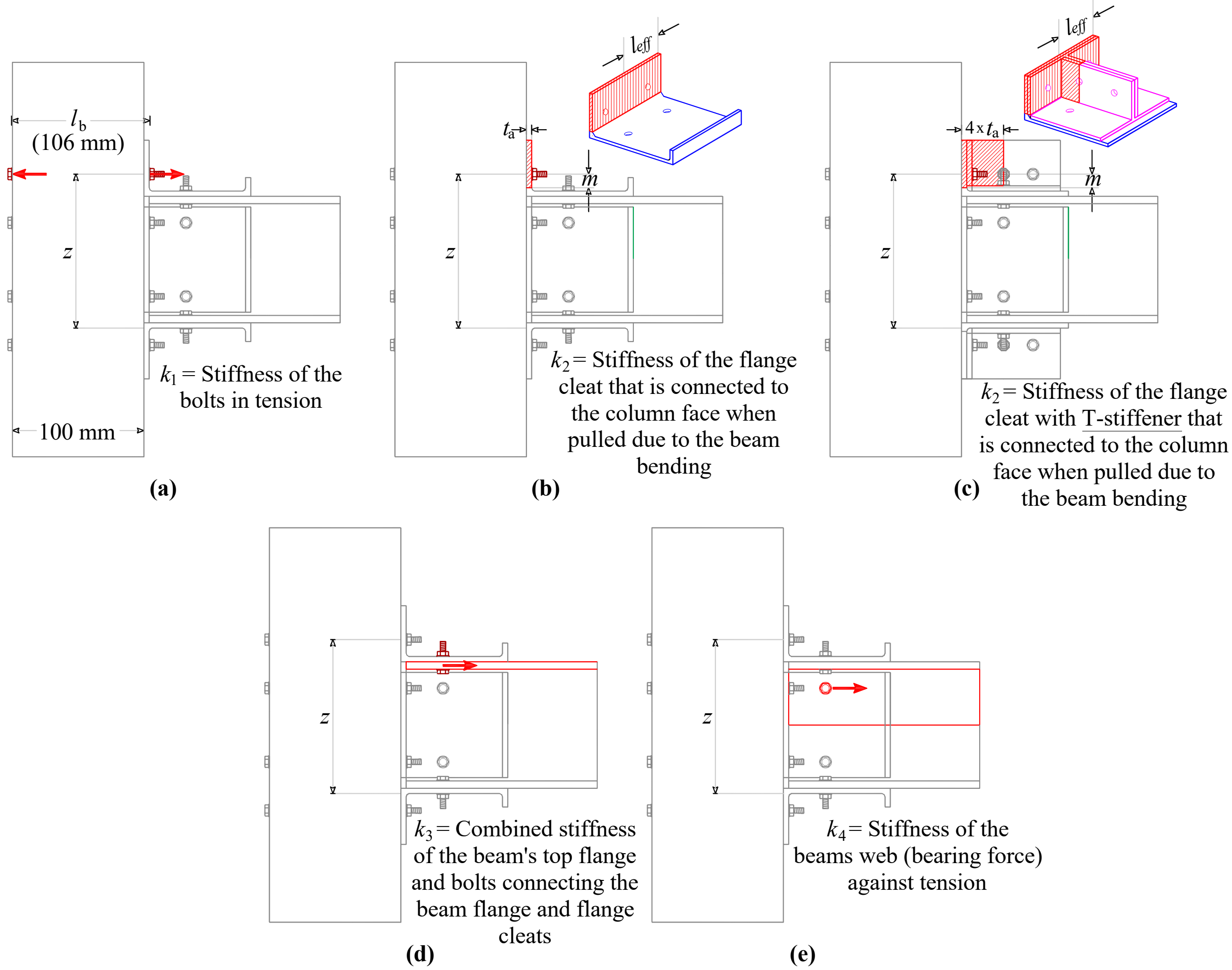

Fig. 10. Stiffness components of the joint component method of initial stiffness determination from Eurocode: (a) k_1 - Stiffness of each row of top rods in tension; (b) k_2 - Stiffness of the top flange cleat (without T-stiffener) in bending; (c) k_2 - Stiffness of the top flange cleat (with T-stiffener) in bending; (d) k_3 - Stiffness of the beam's top bolts in shear; (e) k_4 - Beam's web portion in tension

The Eurocode classified the joint stiffness into twenty different components (Section 6 and Table 6.1 of BS EN 1993-1-8:2005), out of which the following components were selected for concrete-filled columns connected with beam using flange and web cleats (appropriate ones for the present study), namely: (i) stiffness of each row of top rods in tension (bolts connecting the column and top flange cleat - Fig. 10a) as per Eq. (1), denoted as k_1; (ii) stiffness of the top flange cleat in bending as per Eq. (2) (Figs. 10b and 10c), denoted as k_2; (iii) stiffness of the beam's top bolts in shear in Eq. (3), denoted as k_3 (bolts connecting the top flange cleat and top flange of the beam -

Fig. 10d); (iv) beam's web portion in tension (pulling force at the web cleat bolt connection location) as per Eq. (5) (Fig. 10e), denoted as k_4. As the above stiffness components k_1 to k_4 are acting simultaneously (stiffness in series), the total rotational stiffness (k_j) of the joint was calculated using the equivalent stiffness expression Eq. 6. It should be noted that the contributions of the column web and flange stiffness were not incorporated in the present study as the column was filled with concrete and has not deformed until failure as shown in Fig. 5f. In addition, the contribution of the bottom flange cleat was also not considered as it starts acting against the rotation of the beam only after the initial loading or after the failure of the top flange cleat, and theoretically the beam's axis of rotation lies at the bottom flange cleat for the cantilever beam tested in the present study, thus the web cleat also failed in pulling (tension) of the top portion (crack begins at the top of the web cleat and propagates to the bottom).

Stiffness of each row of top rods in tension (k_1)

$$k_1 = \frac{1.6\ A_S\ E_S}{L_b} \quad \text{(Eq. 1)}$$

The stiffness of the bolts connecting the column and top flange cleat is determined using the simple mechanics expression for calculating the stiffness of the bar in tension, Eq. (1) simulates the same. In Eq. (1), A_s is the cross-section area of the bolts in a single row, E_s is the Young's modulus of the bolt (stainless steel), and L_b is the elongation length (length between two ends of the bolts plus the two washers length subtracting thickness of the bolts). Fig. 10a illustrates the force direction of this stiffness and each parameter.

Stiffness of the top flange cleat in bending (k_2)

$$k_2 = \frac{0.9\ l_{eff}\ t_a^3\ E_{t,T}}{m^3} \quad \text{(Eq. 2)}$$

The stiffness of the flange cleat leg that is connected to the column face when pulled by the other leg due to the beam bending and this stiffness is associated with the bolts in tension (k_1). Where the l_{eff} is the effective length of the flange cleat, t_a of the thickness of the flange cleat, $E_{t,T}$ is the tensile modulus of the GFRP flange cleat in a transverse direction (in the direction of the beam), and m is the flat distance of the flange cleat connected to the column face (bending lever arm - flange length of the connecting leg) as depicted in Fig. 10b according to Eurocode. As the Eurocode's joint component method does not have a separate stiffness calculation procedure for the newly introduced T-stiffener connection configuration, the influence of T-stiffener to the top flange cleat against bending is incorporated by increasing the thickness of the flange cleat by four times the actual thickness, that is t_a = 16 mm instead 4 mm flange cleats in specimens T4-4e1-UL-T and T4-8e1-UL-T (Fig. 10c).

Stiffness of the beam's top bolts in shear (k_3)

$$k_3 = \frac{1}{\frac{1}{k_b} - \frac{1}{k_{plate}}} \qquad \text{(Eq. 3)}$$

This is the combined stiffness of the top flange plate in the PFRP beam and bolts connecting the beam flange and flange cleats, when the beam is bending the resistance is provided by the connecting bolts together with the flange cleat bending as shown in Fig. 10d. Where k_b = stiffness of the bolted connection obtained from the double lap connection test, for the present study the stiffness of the 6 mm bolt and 4 mm thick plate is obtained from the authors previous double lap single bolt connection testing work (Selvaraj et al. 2023).

$$k_{plate} = \frac{E_{t,Lf} \ A_{flange}}{l_{ff}} \qquad \text{(Eq. 4)}$$

where $E_{t,Lf}$ is the tensile modulus of the beam flange in the longitudinal direction, A_{flange} is the effective area for the single bolt, l_{ff} is the free length of the beam flange (unrestrained length) can be calculated as the distance from the end of top flange cleat to the loading point divided by 2.

Beam's web portion in tension (k_4)

$$k_4 = \frac{E_{t,Lw}\ A_{web}}{l_{fw}} \quad \text{(Eq. 5)}$$

The Eurocode suggests that when the beam webs are connected to columns by web cleats, the top portion of the beam's web will have a bearing stiffness (Fig. 10e), therefore this can be determined using a very similar approach in Eq. 4, nevertheless, the parameters are taken according to the web. Where $E_{t,Lw}$ is the tensile modulus of the web of the beam in the longitudinal direction, A_{web} is the effective area for a single bolt in the web (only the top portion of the web in tension during the initial loading), l_{fw} is the free length of the beam's flange (unrestrained length) can be calculated as the distance from the end of web cleat to the loading point divided by 2 (will be equal to l_{ff}).

Table 4: Validation of the joint component method of initial stiffness determination from Eurocode

Specimen Nomenclature	$k_{E\text{-}j}$ (kNm/rad)	k_1 (kN/m)	k_2 (kN/m)	k_3 (kN/m)	k_4 (kN/m)	k_j (kNm/rad)	$k_{E\text{-}j}/k_j$
T4 - 4e1 - L - Fig. 2f	48.48	166113.8	4182.2	3687.1	42670.1	39.3	1.23
T4 - 6e1 - L - Fig. 2g	51.52	166113.8	4182.2	3687.1	42670.1	39.3	1.31
T4 - 8e1 - UL - Fig. 2h	47.88	166113.8	4182.2	3687.1	42670.1	39.3	1.22
T4 - 8e1 - L - Fig. 2i	54.64	166113.8	4182.2	3687.1	42670.1	39.3	1.39
T9 - 4e1 - L - Fig. 2j	56.62	166113.8	147053.2	3572.7	42670.1	105.0	0.54
T9 - 6e1 - L - Fig. 2k	68.35	166113.8	147053.2	3572.7	42670.1	105.0	0.65
T9 - 8e1 - UL - Fig. 2l	131.50	166113.8	147053.2	3572.7	42670.1	105.0	1.25
T9 - 8e1 - L - Fig. 2m	139.92	166113.8	147053.2	3572.7	42670.1	105.0	1.33
T4 - 4e1 - UL - T - Fig. 2n	146.57	166113.8	267660.0	3534.4	42670.1	118.7	1.23
T4 - 8e1 - UL - T - Fig. 2o	161.93	166113.8	267660.0	3534.4	42670.1	118.7	1.36

Note: Refer to Fig. 10 and the design example in supplementary material for the procedure for the joint component method of initial stiffness determination according to Eurocode.

Overall rotational stiffness of the joint (k_j)

$$k_j = \frac{z^2}{\frac{1}{k_1}+\frac{1}{k_2}+\frac{1}{2k_3}+\frac{1}{k_4}} \quad \text{(Eq. 6)}$$

Where k_j is the overall stiffness of the beam-to-column joint, z is the moment lever arm as depicted in Fig. 10, k_1, k_2, k_3, and k_4 are from Eqs. (1-5). It should be noted that the stiffness of the beam's top bolts in shear (k_3) is multiplied by two as there are two bolts k_3 used for connecting the flange cleat and column.

Validation of the joint component method of initial stiffness determination from Eurocode

Despite the fact that the joint component method of stiffness prediction in Section 6 and Table 6.1 of BS EN 1993-1-8:2005 is developed for steel "Structural joints connecting H or I sections", the comparison between predicted rotational stiffness of the joint (k_j) and stiffness obtained from experiments ($k_{E\text{-}j}$) for PFRP joints shows relatively good agreement (Table 4). However, it should be noted that the predicted rotational stiffness (k_j) of the joints is conservative ($k_{E\text{-}j} > k_j$) for the 8 specimens by an average of 23% but significantly unconservative for 2 specimens by an average of 45%. This may be attributed to the fact that the failure mode and resistance of the connection components are significantly influenced by the end spacing (e_1), but the stiffness design expressions (Eqs. 1-6) do not consider the end spacing as one of the parameters. In addition, it should also be noted that except for the stiffness of the flange cleat in bending (k_2 varying with respect to the thickness of the top flange cleat), all the other stiffness components k_1, k_3, and k_4 are the same for all the specimens as the parameters incorporated are same such as $E_{t,Lw}$, A_{web}, l_{fw}, l_{ff}, A_{flange}, $E_{t,Lf}$, A_s, E_s and L_b. The predicted values of k_j may be even accurate if the other parameters such as e_1, e_2, and minimum fiber architecture limitations are included in the design. With the current results, it can be concluded that the Eurocode method of stiffness prediction is conservative for the PFRP beam-to-column connections with an end distance equal to $8d_b$. The stiffness prediction of the tested beam-to-column joint specimen T9-8e_1-L is demonstrated in the form of a design example in supplementary material for ease of understanding of the reader and design engineers.

Conclusions

An experimental investigation was carried out on the glass PFRP beam-to-column joints with varying design parameters. The initial joint stiffness, ultimate moment, first failure, and failure mode patterns were analyzed based on design parameters such as end distance, cleat thicknesses, and additional T-stiffeners. The structural response of the connection component indicated that the following: (i) the increase in thickness of the connecting components (flange and web cleats) does not improve the connection behavior proportionally; (ii) the thicker PFRP profiles like 9 mm cleat angles should have adequate end distance (e_1) and more bidirectional layers to avoid sudden cracking; (iii) more load transfer connecting element is required for delaying the brittle failure (improve the initial stiffness), (iv) the fiber architecture of the PFRP plates significantly influence the overall response of the joint. The additional T-stiffeners with the top and bottom flanges significantly increased the stiffness of the joint and improved the failure modes. Particularly, the introduction of the T-stiffeners delayed the first failure beyond the serviceability limits which is a safety factor in the design of PFRP structures. In the present study, the initial stiffness of the PFRP beam-to-column joint was determined using the "joint component" method from Eurocode which is modified according to the PFRP connection configuration, load transfer, and failure modes. The predicted rotational stiffness (k_j) of the joints is conservative ($k_{E\text{-}j} > k_j$) for the 8 specimens by an average of 23%, but significantly unconservative for 2 specimens by an average of 45%. This is due to the fact that the failure mode and resistance of the connection components are significantly influenced by the end spacing (e_1), but the stiffness design expressions do not consider the end spacing as one of the parameters. The predicted values of k_j may be even accurate if the other parameters such as e_1, e_2, and minimum fiber architecture limitations are included in the design. With the present results, it can be concluded that the Eurocode method of stiffness prediction is conservative for the PFRP beam-to-column connections with an end distance equal to $8d_b$. A design example is included for ease of understanding and application. The conclusion drawn from this research is applicable to the beam-to-column joints that are made from PFRP profile with similar fiber weight fraction ratio and architecture.

Data Availability Statement

Some or all data, models, or codes that support the findings of this study are available from the corresponding author upon reasonable request

Acknowledgments

The research work presented in this paper was supported by the Research Grants Council of the Hong Kong Special Administrative Region, China - Theme-based Research Scheme (Project No. T22-502/18-R).

References

Abdelkerim, D.S., Wang, X., Ibrahim, H.A. and Wu, Z., 2019. Static and fatigue behavior of pultruded FRP multi-bolted joints with basalt FRP and hybrid steel-FRP bolts. Compos. Struct., 220, pp.324-337.

Abdelkerim, D.S., Wang, X., Ibrahim, H.A. and Wu, Z., 2020. Effect of connection techniques on the static and fatigue performance of pultruded basalt FRP multibolted joints. J. Compos. Constr., 24(5), p.04020046.

American Society of Civil Engineers (ASCE), (2010). Pre-standard for load & resistance factor design (LRFD) of pultruded fiber reinforced polymer (FRP) structures (Final). 2010.

American Society of Civil Engineers (ASCE), (2011). Design for FRP Composite Connections, ASCE Manuals and Reports on Engineering Practice MOP#102, ISBN: 978-0-7844-0612-0, 2011.

ASTM. Standard test method for tensile properties of polymer matrix composite materials. ASTM D3039/D3039M. West Conshohocken, PA: ASTM, 2014.

ASTM. Standard test methods for constituent content of composite materials. ASTM D3171. West Conshohocken, PA: ASTM, 2015.

Bank, L.C., Mosallam, A.S. and Gonsior, H.E., 1990. Beam-to-column connections for pultruded FRP structures. In Serviceability and Durability of Construction Materials (pp. 804-813).

Bank, L.C. and Mosallam, A.S., 1992. Creep and failure of a full-size fiber-reinforced plastic pultruded frame. Compos. Eng, 2(3), pp.213-227.

Bank, L.C., Mosallam, A.S. and McCoy, G.T., 1994. Design and performance of connections for pultruded frame structures. Journal of reinforced plastics and composites, 13(3), pp.199-212.

Bank, L.C., (2023). Reflections on 50 Years of Pultruded Fiber-Reinforced Polymer Materials in Structural Engineering. J. Compos. Constr., 27(5), p.02523001.

Bass, A.J. and Mottram, J.T., 1994. Behaviour of connections in frames of fibre-reinforced-polymer section. Struct. Eng., 72(17), pp.280-284.

CEN, Eurocode 3 (BS EN 1993-1-8:2005): Design of Steel Structures - Part 1–8: Design of Joints, EN 1993-1-8, Brussels, 2005

CEN/TS 19101. Design of Fibre-polymer composite structures, Technical committee, European Commission, 2020.

Clarke, J. L., ed. Structural design of polymeric composites- EUROCOMP design code and handbook. E & FN Spon, London, 1991.

CNR. Guide for the design and construction of structures made of FRP pultruded elements, CNR - Advisory Committee on Technical Recommendations for Construction and National Research Council of Italy, CNR-DT 205/2007, Rome,2008.

Coelho, A.M.G. and Mottram, J.T., "A review of the behaviour and analysis of bolted connections and joints in pultruded fibre reinforced polymers", Materials & Design, 74, pp.86-107, 2015.

El-Badry, M. M., ed. Proc., 2nd Int. Conf. on Advanced Compos. Mat. in Bridges and Struct., Canadian Society for Civil Engineering, Montreal, 1996.

Ellingwood, B.R., "Toward load and resistance factor design for fiber-reinforced polymer composite structures". J. Struct. Eng., 129(4), pp.449-458, 2003.

European Union (EU). Prospect for new guidance in the design of FRP. EUR 27666. Publications Office of the European Union; Ispra (Italy), JRC99714, 2016.

EXTREN. Fiberglass structural shapes design manual. Strongwell, Bristol, Va, 1989.

Feng, P., Li, Z., Wang, J. and Liu, T., "Novel joint for pultruded FRP beams and concrete-filled FRP columns: Conceptual and experimental investigations", Compos. Struct., 287, p.115339, 2022.

Fiberline design manual for structural profiles in composite materials. Fiberline Composites A/S, Kolding, Denmark, 1995.

FprCEN/TS 19101. Design of Fibre-Polymer Composite Structures. European Committee for Standardization, CEN/TC 250, 2022.

Gand, A.K., Chan, T.M. and Mottram, J.T., 2013. Civil and structural engineering applications, recent trends, research and developments on pultruded fiber reinforced polymer closed sections: a review. Frontiers of Structural and Civil Engineering, 7, pp.227-244.

Lawler, N. and Polak, M.A., 2011. Development of FRP shear bolts for punching shear retrofit of reinforced concrete slabs. J. Compos. Constr., 15(4), pp.591-601.

Luo, F.J., Huang, Y., He, X., Qi, Y. and Bai, Y., 2019. Development of latticed structures with bolted steel sleeve and plate connection and hollow section GFRP members. Thin-Walled Structures, 137, pp.106-116.

Martins, D., Proença, Correia, Gonilha, Arruda, M, Silvestre, N. 2017. Development of a novel beam-to-column connection system for pultruded GFRP tubular profiles. Compos. Struct., 171, pp.263-276.

Martins, D., Gonilha, J., Correia, J.R. and Silvestre, N., 2021a. Exterior beam-to-column bolted connections between GFRP I-shaped pultruded profiles using stainless steel cleats. Part 1: Experimental study. Thin-Walled Struct, 163, p.107719.

Martins, D., Gonilha, J., Correia, J.R. and Silvestre, N., 2021b "Exterior beam-to-column bolted connections between GFRP I-shaped pultruded profiles using stainless steel cleats, Part 2: Prediction of initial stiffness and strength", Thin-Walled Struct, 164, p.107762.

Martins, D., Gonilha, J., Correia, J.R. and Silvestre, N., "Monotonic and cyclic behaviour of cuff beam-to-column connection system for tubular pultruded GFRP profiles," Eng. Struct., 247, p.113165, 2021c.

Martins, D., Gonilha, J., Correia, J.R. and Silvestre, N., 2021d. Monotonic and cyclic behaviour of a stainless steel cuff system for beam-to-column connections between pultruded I-section GFRP profiles. Engineering Structures, 249, p.113294.

Martins, D., Gonilha, J., Correia, J.R., Silvestre, N., Guerreiro, L. and Branco, F., 2023. Monotonic and cyclic sway behaviour of 2-dimensional frames made of pultruded GFRP I-section profiles. Structures (Vol. 55, pp. 2461-2477).

Mosallam, A.S., Abdelhamid, M.K. and Conway, J.H., 1994. Performance of pultruded FRP connections under static and dynamic loads. Journal of Reinforced Plastics and Composites, 13(5), pp.386-407.

Mottram, J.T. and Zheng, Y., 1999a "Further tests on beam-to-column connections for pultruded frames: web-cleated". J. Compos. Constr., 3(1), pp.3-11.

Mottram, J.T. and Zheng, Y., 1999b "Further tests of beam-to-column connections for pultruded frames: flange-cleated". J. Compos. Constr., 3(3), pp.108-116.

Mottram, J.T. and Zheng, Y., 1996. "State-of-the-art review on the design of beam-to-column connections for pultruded frames". Compos. Struct., 35(4), pp.387-401.

Mottram, J. T. (1994). ''Connection tests for pultruded frames.'' Civ. Engrg. Group, Res. Rep. CE47, Dept. of Engrg., University of Warwick, Coventry, UK.

Mottram, J. T. (1996). ''Nominally pinned connections for pultruded frames.'' Structural design of polymer composites-EUROCOMP design code and handbook, J. L. Clarke, ed., E & FN Spon, London, 703–718.

Nguyen, T.T., Chan, T.M. and Mottram, J.T., 2013. Influence of boundary conditions and geometric imperfections on lateral–torsional buckling resistance of a pultruded FRP I-beam by FEA. Compos. Struct., 100, p.233-242.

Nguyen, T.T., Chan, T.M. and Mottram, J.T., 2014. Lateral-torsional buckling resistance by testing for pultruded FRP beams under different loading and displacement boundary conditions. Compos. Part B: Eng., 60, p.306-318.

Nguyen, T.T., Chan, T.M. and Mottram, J.T., 2015. Lateral–Torsional Buckling design for pultruded FRP beams. Compos. Struct., 133, p.782-793.

Qureshi, J. and Mottram, J.T., 2013. Behaviour of pultruded beam-to-column joints using steel web cleats. Thin-Walled Struct, 73, pp.48-56.

Qureshi, J. and Mottram, J.T., "Response of beam-to-column web cleated joints for FRP pultruded members", J. Compos. Constr., 18(2), p.04013039, 2014.

Qureshi, J. and Mottram, J.T., "Moment-rotation response of nominally pinned beam-to-column joints for frames of pultruded fibre reinforced polymer". Constr Build Mater, 77, pp.396-403, 2015.

Qureshi, J., Nadir, Y. and John, S.K., 2020. Bolted and bonded FRP beam-column joints with semi-rigid end conditions. Compos. Struct., 247, p.112500.

Selvaraj, S., Chan, T.M. and Young, B., "Influence of geometry on failure modes of PFRP single bolted connections, Eng. Struct., 274, p.115078, 2023.

Selvaraj, S. and Madhavan, M., (2019) "Strengthening of laterally restrained steel beams subjected to flexural loading using low-modulus CFRP", J. Perform. Constr. Facil., 33(3), p.04019032.

Selvaraj, S. and Madhavan, M., (2020) "Design of steel beams strengthened with low-modulus CFRP laminates", J. Compos. Constr., 24(1), p.04019052.

Singamsethi, S.K., LaFave, J.M. and Hjelmstad, K.D., 2005. Fabrication and testing of cuff connections for GFRP box sections. J. Compos. Constr., 9(6), pp.536-544.

Smith, S.J. Parsons, I.D., Hjelmstad, K.D. An experimental study of the behavior of connections for pultruded GFRP I-beams and rectangular tubes, Compos. Struct. 42 (1998) 281–290.

Smith, S.J., Parsons, I.D. and Hjelmstad, K.D., 1999. Experimental comparisons of connections for GFRP pultruded frames. J. Compos. Constr., 3(1), pp.20-26.

Teng, J.G., Xiang, Y., Yu, T. and Fang, Z., 2019. Development and mechanical behaviour of ultra-high-performance seawater sea-sand concrete. Adv. Struct. Eng., 22(14), pp.3100-3120.

Turvey, G.J., 2000. Moment–rotation tests on bolted end connections in pultruded GRP beams–tests with stainless steel cleats and an assessment of their performance relative to GRP cleats.

Turvey, G.J. and Cooper, C., 2004. Review of tests on bolted joints between pultruded GRP profiles. Pro. Institution of Civil Engineers-Structures and Buildings, 157(3), pp.211-233.

Uy, B., Patel, V., Li, D. and Aslani, F., 2017, February. Behaviour and design of connections for demountable steel and composite structures. Structures (Vol. 9, pp. 1-12). Elsevier.

Xiao, X., Xie, L., Wang, Y., Dai, N. and Yin, X., 2022. Monotonic loading performance of GFRP beam-column joints connected with slotted-hole bolts. Plos one, 17(7), p.e0272136.

Zhang, Z.J., Bai, Y. and Xiao, X., 2018. Bonded sleeve connections for joining tubular glass fiber-reinforced polymer beams and columns: experimental and numerical studies. J. Compos. Constr., 22(4), p.04018019.